WATER RESOURCES RESEARCH, VOL. 36, NO. 6, PAGES 1467–1479, JUNE 2000

Submarine groundwater discharge into the sea and associated nutrient transport in a sandy beach

Yusuke Uchiyama,[1] Kazuo Nadaoka,[2] Peter Rölke,[2] Kumiko Adachi,[3] and Hiroshi Yagi[4]

Abstract. Submarine groundwater discharge (SGWD) and associated nutrient fluxes at Hasaki Beach along the Kashima coast in Japan were investigated through field measurements and numerical simulations. The field data indicate that (1) groundwater has higher concentrations of land-derived nutrients than seawater and river water; (2) microbial activity near the shoreline is likely to induce mineralization, reduction, and oxidation of nitrogen and phosphorus; and (3) in the portion of the aquifer underlying coastal forest, nitrate is appreciably reduced. A numerical model incorporating effects of water table and tidal fluctuations was developed to evaluate SGWD. Assuming that the aquifer consists of homogeneous sandy soil, the simulation results show that the nutrient flux due to SGWD is less than that of Tone River discharge. The nutrient flux via groundwater seepage is considered to be a minor component of primary productivity in the surf zone.

1. Introduction

Coastal marine ecosystems are affected by dissolved nutrient inputs from circulating offshore water, river runoff, and groundwater seepage. The regional nutrient budget also includes atmospheric deposition, fertilizer application, wastewater treatment plant discharge, livestock waste, and remineralization of organic matter in sediment. Among these sources the effects of groundwater on marine environments are not as well known as those of river water and offshore water. Groundwater containing inorganic nutrients can have a significant influence on coastal ecosystems, especially when nutrient concentrations are high or relative contribution of submarine groundwater discharge (SGWD) is large. Owing to nutrient leaching from surface-applied fertilizers, groundwater usually has a higher concentration of inorganic nutrients than does seawater. Therefore even low rates of SGWD often need to be accounted for in the nutrient budget for a coastal ecosystem.

Ecologists have not paid much attention to groundwater as a source of inorganic nutrients for coastal marine ecosystems. *Kohout* [1964] and *Kohout and Kolipinski* [1967] were the first investigators to study the importance of fresh groundwater seepage into the sea. Their studies were conducted along the shore of Biscayne Bay, Florida, and showed a definite relationship between biological zonation and groundwater discharge into the bay. *Johannes* [1980] pointed out that on many coasts, groundwater discharge can provide significant amounts of nutrients. *Sutcliff* [1972] demonstrated a significant positive correlation between the rate of nutrient discharge and commercial fish yields. Various reports documented that groundwater seepage has a major influence on nutrient levels on the Guam fringing reef flat [*Marsh*, 1977], Discovery Bay, Jamaica [*D'Elia et al*., 1981], and great South Bay, New York [*Capone and Bautista*, 1985]. More recently, *McLachlan and Illenberger* [1986] and *Simmons* [1992] presented measurements showing quantitatively the importance of nutrient fluxes from coastal aquifers to the marine environment.

SGWD occurs where an aquifer is connected hydraulically with the sea and the groundwater head is above sea level; such conditions are very common [e.g., *Emery and Foster*, 1948; *Manheim*, 1967]. Fresh groundwater flows out to the sea through a narrow seepage face as shown in Figure 1 [e.g., *Glover*, 1959]. The discharged groundwater is brackish toward the seaward edge of the aquifer because of entrainment of salt water from the diffusion zone [*Cooper*, 1959]. The width of the discharge zone (seeping face) is believed to be nearly proportional to the volume of freshwater flow [*Glover*, 1959]. An underlying saltwater wedge typically intrudes beneath the freshwater aquifer along marine coastlines. This wedge impedes the downward mixing of lighter groundwater and thus magnifies the tendency for groundwater from unconfined aquifers to discharge close to the shore. Since the beach water table rises and falls in response to the tides but tends to lag behind the tides [*Emery and Foster*, 1948], the discharge zone may extend above the mean seawater level at low tides. The velocity field in a coastal aquifer appears to be complicated by the influence of the saltwater wedge. Previous studies have not taken into account the spatially variable flow field. Since it is extremely difficult to measure the flow in the aquifer directly, piezometers are often used to obtain data on the head field from which the flow patterns are inferred [e.g., *Neilsen and Dunn*, 1998]. On the other hand, the Darcy's law and Ghyben-Herzberg relationships have been used to calculate the velocity approximately [*Raghunath*, 1982; *McLachlan and Illenberger*, 1986]. Previous estimates of SGWD have generally yielded worldwide figures in the range 0.01–10% of total discharge into the sea [e.g., *Church*, 1996; *Johannes*, 1980]. Nevertheless,

[1]Marine Environment Division, Port and Harbour Research Institute, Nagase, Yokosuka, Japan.
[2]Graduate School of Information Science and Engineering, Tokyo Institute of Technology, O-okayama, Meguro-ku, Tokyo.
[3]National Research Institute of Fisheries Engineering, Ebidai, Hasaki, Ibaraki, Japan.
[4]Department of Civil Engineering, Tokyo Institute of Technology, O-okayama, Meguro-ku, Tokyo.

Paper number 2000WR900029.
0043-1397/00/2000WR900029$09.00

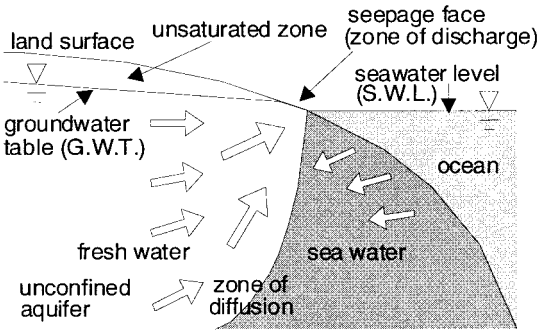

Figure 1. Conceptual illustration of groundwater flow in an unconfined coastal aquifer.

Moore [1996] and *Church* [1996] inferred from ^{226}Ra measurements in coastal waters that SGWD into the South Atlantic Bight might amount to a flux equivalent to 40% of the total flow entering the sea from adjacent rivers. We are unsure whether the figure of 40% is precise; however, the uncomplicated calculations might lead to overestimates of SGWD, as discussed by *Younger* [1996].

This paper reports comprehensive and spatially detailed assessment of submarine groundwater discharge, and the associated nutrient transport, at Hasaki Beach facing the Kashima Sea in Japan. Additionally, in order to calculate the nutrient fluxes we develop a numerical model including the effects of water table and tidal fluctuations to evaluate the velocity field in the coastal aquifer.

2. Study Site

Hasaki Beach, where the field measurements were conducted, is located along the Kashima coast in Japan facing the Pacific Ocean (see Figure 2). An uninterrupted sandy beach extends 16 km from the Tone River mouth to the Kashima port. Groundwater observation wells were installed near the Hasaki Oceanographical Research Station (HORS), the observatory facility of the Port and Harbor Research Institute, and 12 km north of the river mouth. The Tone River is one of the longest rivers in Japan (322 km) and has the largest drainage basin (15,760 km^3).

Hasaki Beach is flanked by a 150–500 m surf zone on the seaward side and a dune 120 m from the shoreline. The dune is covered with sparse coastal grasses. Pine trees, which are ~5–10 m high at present, have been planted to stabilize the area behind the dune. Next to the pine tree strip (100 m wide), a street runs along the coast from the Tone River mouth in the south to the Kashima port in the north. Landward of this street, a highly agricultural area begins. The agricultural area, which is schematically indicated in Figure 2, is 4–5 km wide, mostly covered with paddy fields. The only unaltered area in Hasaki is the narrow beach and dune strip.

The geological history of the Kanto plain, on which the study area is located, is characterized by transgressions and regressions, often caused by tectonic and volcanic activities. Alluvial and marine terraces generally occur in the Kanto plain. The Hasaki area at the eastern boundary of the Kanto plain near the Tone River mouth consists of sandy marine and alluvial deposits, laid down in river channels or on floodplains [*Kimura et al.*, 1991]. These deposits are composed of unconsolidated sand and gravel. River deposits generally have characteristic textural variability that causes appreciable heterogeneity in the distribution of hydraulic properties. The bedded character of fluvial deposits imparts a strong anisotropy; horizontal conductivities are typically 2–10 times larger than vertical conductivities [*Freeze and Cherry*, 1979; *Apello and Postma*, 1993].

According to the survey during drilling of the observation wells, the soil in Hasaki appears to be nearly homogeneous and highly permeable sand. Measured sand particle diameters and the values of the estimated hydraulic conductivity are in the range of 0.125–0.25 mm and 10^{-3}–10^{-2} cm/s, respectively. The groundwater aquifer at Hasaki Beach is likely to be unconfined. Although no aquicludes or relatively impermeable strata were encountered in boreholes drilled in this study, data from other wells near the coastal area indicate that an aquiclude exists ~30–40 m below the ground surface (Figure 3). No information is available about deeper confined aquifers in the study area. Here we considered that there is only the single unconfined aquifer composed of homogeneous fine sand. This assumption is only approximately valid over monitored section based on drilling results.

3. Methods

3.1. Field Observation

Field measurements were conducted from August 7 to December 12 in 1997. A cross section showing locations of 17 observation wells installed at Hasaki Beach is indicated in Figure 4. Three of the wells were placed near the shoreline

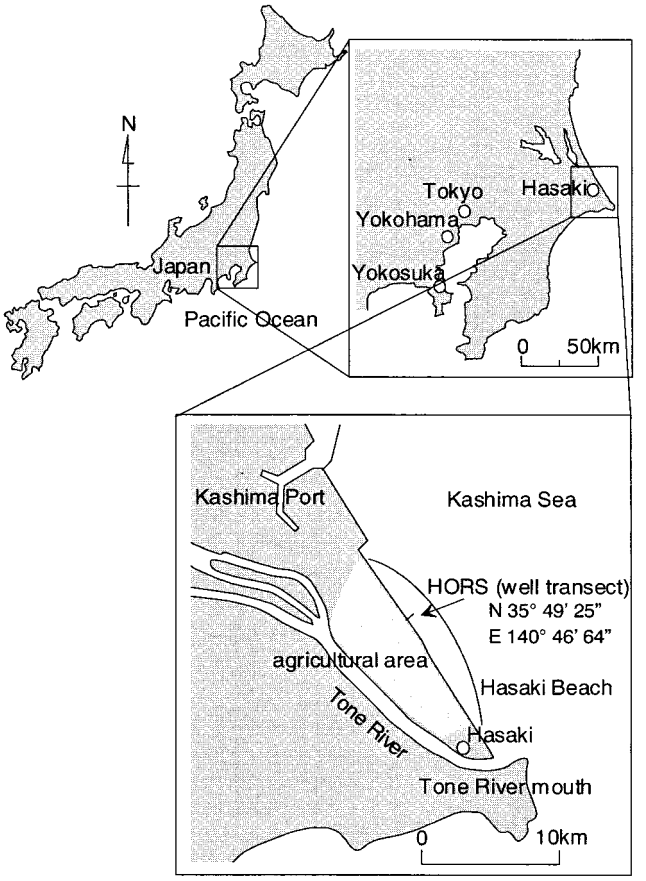

Figure 2. Location of the field survey in the Kashima coast of Japan.

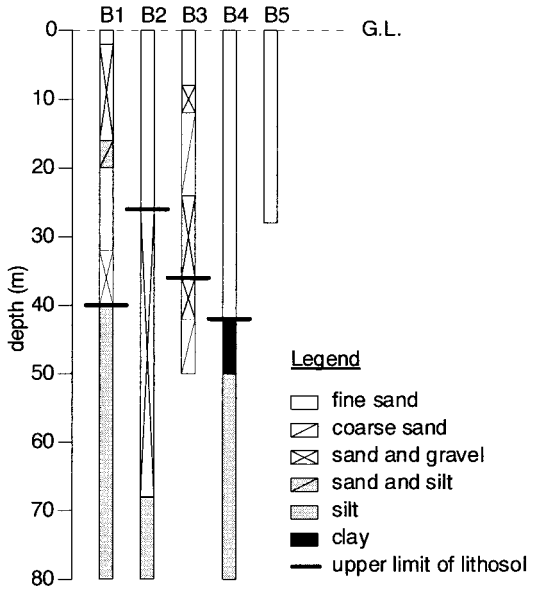

Figure 3. Geological columnar section. B1–B4 are 1–5 km distant from HORS; B5 is station 6.

with datum level (DL) +2.2 m (referred to as station 1) and the others (i.e., stations 2–6) were installed landward of station 1. DL means the datum level of Hasaki Fishery Port and is equivalent to the low water level. High water level approximately corresponds to the ground level at station 1. A PVC casing with a diameter of 125 mm was driven into the desired depths of the sandy soil as well points. The deepest drilling reached 30 m below the land surface or 22 m below the groundwater table.

Clusters of two to five wells screened at different depths were installed at five of the six stations (Figure 4). The screen material is tetrafluoroethylene with slot size of 0.07 mm. Two different depths were considered in the upgradient area and five different depths near the shoreline. The screen lengths were extended in inland wells to 8–10 m long to acquire average results for a large groundwater layer. The ground levels (GL), averaged groundwater table (GWT), and top levels of the wells (WL) measured from DL are also displayed in Figure 4.

Samples of the groundwater in the coastal aquifer were taken on August 7 and 22, September 5 and 25, October 9 and 31, and December 12 by using a bailer sampler [e.g., *Rigg and Hatheay*, 1988; *Nielsen and Yeates*, 1985] made of glass with a diameter of 40.0 mm and a length of 50.0 cm. Additional samplings at stations 1–3 were made on August 26 and December 1. These samples were stored in plastic bottles (250 mL) and brought back to a laboratory for salinity measurements in a few hours. The samples were also purged with membrane filters and stored in polyprophylene tubes (20 mL) which were promptly frozen for preservation. Subsequently, we analyzed the samples with a TRAACS-800 autoanalyser (Bran and Ruebbe Company) to determine the concentrations of NO_2^-, $NO_3^- + NO_2^-$, NH_4^+, PO_4^{3-}, and SiO_2. Dissolved oxygen (DO) was measured before the sampling with a battery-operated instrument (YSI Company) on October 31 and December 12. In addition, water samples were collected from the Tone River mouth and from the beach shoreline. With these data we could compare the nutrient concentrations in the groundwater, river water, and seawater. Water table elevations were also monitored every 10 min over 5 months from August to December in 1997 at three locations, in the observation wells of stations 4–6, with pressure gages (Diver, Eijkelkamp Company). Tide levels were observed at the tip of the observatory pier of HORS.

3.2. Numerical Simulation

Although measurements of hydraulic head are relatively easy to collect, it is generally difficult or impossible to measure

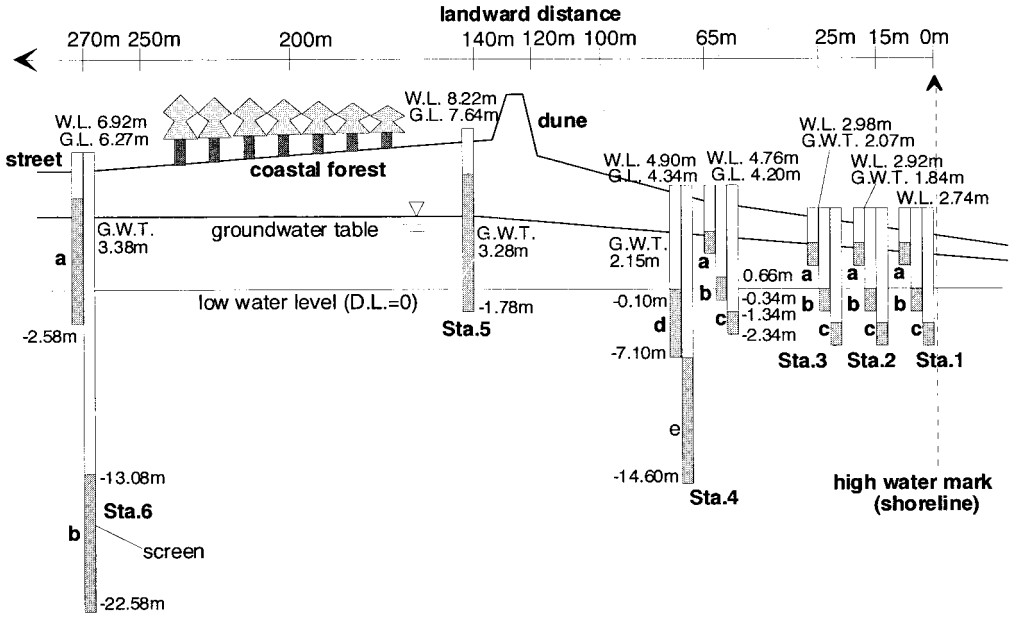

Figure 4. Location of the observation wells near HORS. Station 1 is located at the high water mark. DL is the datum level of Hasaki Fishery Port, being equivalent to low water level. The ground levels (GL), averaged groundwater table (GWT), and top levels of the wells (WL) measured from DL are also displayed.

the velocity field in aquifers. Therefore we developed a numerical model to calculate the detailed velocity field in the coastal aquifer. The measured tide levels and groundwater table elevations were used as boundary conditions in the model.

During the ebb tide the beach water table may become decoupled from the ocean, resulting in the formation of a seepage face where groundwater outcrops on the intertidal profile [e.g., *Nielsen*, 1990; *Turner*, 1993]. The groundwater flow field in the intertidal zone is important for evaluating material transport due to SGWD as shown in Figure 1. Since unsaturated layers are attributed to the pressure potential distribution near the groundwater table including the intertidal zone, the numerical model should be based on the Richards equation for saturated-unsaturated flow [*Richards*, 1931]. In addition, density effects induced by intrusion of saline seawater are not negligible in analyzing flow in a coastal aquifer.

Pinder and Cooper [1970] demonstrated the movement of the saltwater front in confined coastal aquifers by using a numerical model. Their model used a steady groundwater flow equation and a time-dependent advection-dispersion equation for salinity. *Segol et al*. [1975] employed this model for a computation of steady flow in unconfined aquifers. Others incorporated Richards equation for unsteady flow [e.g., *Kohno et al*., 1983]. Although the previous works have treated transient flow related to surface recharge and drainage in coastal aquifers, unsteady flow due to the fluctuating tides and waves has not been simulated previously using this framework. *Li et al*. [1997a] recently presented a boundary element method model solving the Laplace equation for saturated flow in an unconfined coastal aquifer. They incorporated the capillary effects derived from the approximate solution of the one-dimensional Richards equation [*Parlange and Brutsaert*, 1987] into the model and demonstrated beach water table fluctuations due to tides and waves [*Li et al*., 1997a, b]. In their model, however, spatial distribution of hydraulic conductivity could not be included. Additionally, they neglected the effect of density-driven flow caused by the presence of salt water.

Assuming that the aquifer studied here is isotropic and including the variation of pressure potential due to the change of groundwater density, we can obtain the Darcian flow equation as [*Pinder and Cooper*, 1970; *Pinder and Gray*, 1977]

$$\mathbf{q} = -K(\psi)\ \mathrm{grad}\left\{\psi + \left(\frac{\rho}{\rho_f}\right)z\right\}, \tag{1}$$

where x and y are the longitudinal and transverse coordinates, z is the vertical coordinate, $\mathbf{q} = (q_x, q_y, q_z)$ is the Darcian velocity vector, K is the hydraulic conductivity, ψ is the pressure potential (or matric potential in the unsaturated zone), ρ is density of mixed fluid, and ρ_f is the density of fresh water. Although we assume the aquifer to be homogeneous in this study, K may be varied spatially and temporally in the model.

The Richards equation for saturated-unsaturated groundwater flow, which requires no special treatment of the groundwater table, is derived from (1) and mass conservation of pore water [*Richards*, 1931]

$$[C_w(\psi) + \beta_0 S]\frac{\partial\psi}{\partial t} = \frac{\partial}{\partial x}\left(K\frac{\partial\psi}{\partial x}\right) + \frac{\partial}{\partial y}\left(K\frac{\partial\psi}{\partial y}\right) + \frac{\partial}{\partial z}\left(K\frac{\partial\psi}{\partial z} - \frac{\rho}{\rho_f}K\right), \tag{2}$$

where $C_w(\psi) \equiv \partial\theta/\partial\psi$ is the slope of the soil water retention curve (or the water capacity), $\theta(\psi)$ is the volumetric water content, t is time, S is the specific storage, and β_0 is a variable. On the assumption that the porosity does not vary with fluctuations of the pressure potential, β_0 is expressed as

$$\beta_0 = \begin{cases} 0 & \cdots \text{ unsaturated} \\ 1 & \cdots \text{ saturated.} \end{cases} \tag{3}$$

If the dispersion in the aquifer is assumed to be homogeneous, the advection-dispersion equation governing a passive and conservative solute (e.g., salinity) is defined as (4):

$$\frac{\partial\theta C}{\partial t} + \frac{\partial(\theta q_x' C)}{\partial x} + \frac{\partial(\theta q_y' C)}{\partial y} + \frac{\partial(\theta q_z' C)}{\partial z} = \frac{\partial}{\partial x}\left(\theta D_{xx}\frac{\partial C}{\partial x}\right) + \frac{\partial}{\partial y}\left(\theta D_{yy}\frac{\partial C}{\partial y}\right) + \frac{\partial}{\partial z}\left(\theta D_{zz}\frac{\partial C}{\partial z}\right), \tag{4}$$

where q_x', q_y', and q_z' are the components of the pore water velocity vector ($q_x' = q_x/\theta_s$, $q_y' = q_y/\theta_s$, $q_z' = q_z/\theta_s$; θ_s is field-saturated volumetric water content). C is the nondimensional solute concentration (e.g., nondimensional salinity). D_{xx}, D_{yy}, and D_{zz} are components of the pore-scale dispersion tensor. The values of θD_{xx}, θD_{yy}, and θD_{zz} are proposed by *Scheidegger* [1961] and *Bear* [1972] as

$$\begin{aligned} \theta D_{xx} &= \alpha_L q_x^2/q_s + \alpha_T q_y^2/q_s + \alpha_T q_z^2/q_s + \theta\nu \\ \theta D_{yy} &= \alpha_T q_x^2/q_s + \alpha_L q_y^2/q_s + \alpha_T q_z^2/q_s + \theta\nu \\ \theta D_{zz} &= \alpha_T q_x^2/q_s + \alpha_T q_y^2/q_s + \alpha_L q_z^2/q_s + \theta\nu, \end{aligned} \tag{5}$$

where q_s is the velocity magnitude ($=(q_x^2 + q_y^2 + q_z^2)^{1/2}$), α_L and α_T are the values of the longitudinal and transversal dispersivity, and ν is the kinematic viscosity of water. The values of α_L and α_T are set to be 2.5 and 0.5 cm according to *Momii et al*. [1986].

The relation between the nondimensional salinity C and the density of mixed fluid ρ is

$$C = (\rho - \rho_f)/(\rho_s - \rho_f), \tag{6}$$

where ρ_s is the density of seawater. Nondimensional concentration C hence is 1.0 for seawater and 0.0 for fresh water.

The hydraulic conductivity $K(\psi)$ in homogeneous and isotropic porous media is constant in the saturated zone; however, it varies in response to the change of the volumetric water content $\theta(\psi)$ in the unsaturated zone. In the present model the relationship between $K(\psi)$ and $\theta(\psi)$ proposed by *Brooks and Corey* [1966] is employed. Ignoring hysteresis and local anisotropy and considering the pressure head ψ as the dependent variable, they derived

$$K = K_s\{(\theta - \theta_r)/(\theta_s - \theta_r)\}^m, \tag{7}$$

where K_s is the saturated conductivity, θ_r is the residual water content, and m is a parameter which is theoretically estimated to be 3.0 by *Irmay* [1954]. The values of K_s and θ_s are experimentally obtained for the sand sampled at the study site (station 4): $K_s = 1.331 \times 10^{-2}$ cm/s, and $\theta_s = 0.3759$. The value of θ_r is set to be 1.0×10^{-3}. While various empirical functions for the retention equation exist, we chose the one proposed by *Tani* [1982] to achieve computational robustness.

$$(\theta - \theta_r)/(\theta_s - \theta_r) = (|\psi/\psi_0| + 1)\ \exp\ (|\psi/\psi_0|), \tag{8}$$

where ψ_0 is the matric potential that gives the maximum value of the water capacity C_w.

The backward Euler scheme was used to solve (1)–(8). It is

Table 1. Hydraulic and Physical Parameters of the System Being Simulated

Parameter	Value
Specific storage S	1.0×10^{-3}
Saturated conductivity K_s, cm/s	1.33×10^{-2}
Density of fresh water ρ_f, g/cm^3	1.0
Density of seawater ρ_s, g/cm^3	1.025
Field-saturated volumetric water content θ_s	0.3759
Residual water content θ_r	1.0×10^{-3}
m	3.0
Longitudinal dispersivity α_L, cm	2.5
Transversal dispersivity α_T, cm	0.5
Matric potential ψ_0, cm H_2O	−100

an iterative numerical scheme employing implicit finite difference formulations. The spatial derivatives in (2) and (4) are represented by centered differences. A computational grid uniformly spaced in all directions was adopted, and the grid sizes were chosen as $\Delta x = \Delta y = 2.0$ m and $\Delta z = 0.5$ m. The successive over relaxation (SOR) method with a relaxation parameter of $\omega = 1.2$ was applied to solve the simultaneous algebraic equations. Computational convergence was judged with tolerances of 1.0×10^{-2} for (2) and of 1.0×10^{-4} for (4). The hydraulic and physical parameters of the system being simulated, which are mentioned above, are summarized in Table 1.

In the computations the x and y axes corresponded to the cross-shore and alongshore directions, respectively. Alongshore variations in ψ and C are not considered, and therefore the present simulations are vertically two-dimensional. Free flux conditions were applied above the water table. Prescribed head $\psi = z_0\rho/\rho_f$, in which z_0 is the vertical distance from the phreatic surface, and concentration ($C = 0.0$ at the landward boundary, and $C = 1.0$ at the seaward boundary) were given as horizontal boundary conditions. Vertical boundary conditions were no-flow and no-flux conditions. The initial values of total potential and concentration at all nodes were set at zero; this meant that the aquifer was filled with immobile fresh water.

4. Results

4.1. Nutrient Concentrations in Groundwater, Seawater, and River Water

Figure 5 represents the time series of NO_3^-, NO_2^-, NH_4^+, PO_4^{3-}, and SiO_2 concentration in the seawater, Tone River water, and groundwater. The groundwater was sampled at stations 6-a and 6-b and was unlikely to have been influenced by seawater. Most values of the nutrient concentrations in groundwater are close to or higher than those in river water and seawater; however, river water is found to have higher ammonium concentrations than groundwater and seawater.

Time series of NO_3^-, NO_2^-, NH_4^+, PO_4^{3-}, and SiO_2 concentration in the groundwater at stations 1-a, 1-b, and 1-c are shown in Figure 6. These stations were situated near the shoreline where nutrient concentrations in the groundwater were affected by seawater. Seasonal variations in nitrite, ammonium, and phosphate concentration were clearly observed at station 1. Such variations, however, were not seen in the inland aquifer, e.g., at station 6. At station 1 the nutrient concentrations were remarkably high in August and September and rapidly decreased. There are several explanations for this seasonal variation that should be considered, including seasonal

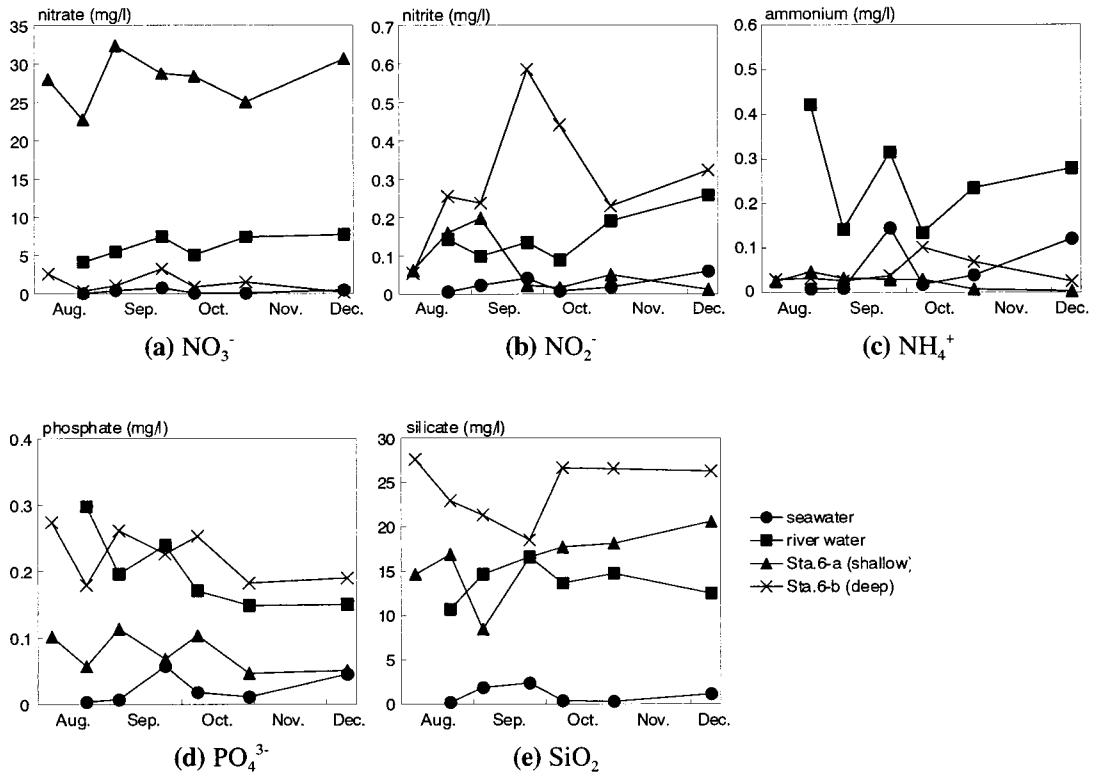

Figure 5. Time series of nutrient concentration in groundwater (stations 6-a and 6-b), seawater, and river water.

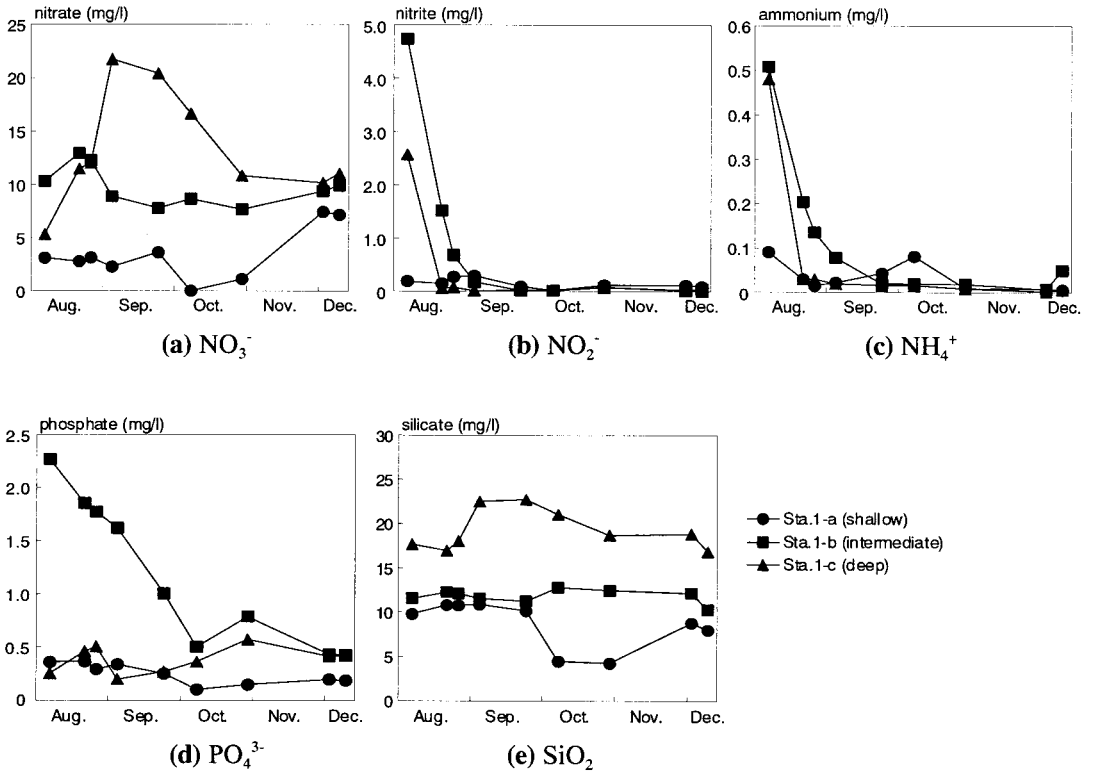

Figure 6. Time series of nutrient concentration in groundwater at the shoreline (stations 1-a, 1-b, and 1-c).

water temperature and water table fluctuations, timing of fertilizer application and irrigation of croplands, nearshore algal blooms, or seasonal change in water beach profile and shoreline position, etc. Further data collections should be performed over a full annual cycle to assess the broader context of the data presented here.

4.2. Verification of the Numerical Model

The numerical model was verified by comparing the computational results with experimental data obtained in a laboratory by *Tamai and Shima* [1967]. The experimental formula for the position of a salt wedge near the shoreline was proposed as

$$C_l(l) = (q_0/\varepsilon K_s)\ \sqrt{(2\varepsilon K_s/q_0)l + 0.55}, \qquad (9)$$

where l is the horizontal distance from the seaward edge of the wedge, C_l is the vertical distance from the l axis to the salt-water wedge, q_0 is the volume flux of the fresh groundwater discharge per unit width from the landward end of the aquifer, and ε is the normalized density difference ($\varepsilon = (\rho_s - \rho_f)/\rho_f = 0.025$). Figure 7 illustrates a definition sketch of (9), in which the values of K_s and Δh were set to be 0.20 cm/s and 10.0 cm.

Figure 8 displays computational results of the velocity field and salinity distribution in the steady state. The position of the interface calculated from (9) is also plotted in Figure 8b. The value of q_0 was estimated to be 1.237 cm^2/s by the numerical simulator. Whereas (9) predicts the salt wedge as a sharp interface, the simulation results showed that a thin mixing zone separates the fresh and saline groundwater. The latter prediction is clearly more realistic. Nevertheless, we can see that the numerical model is capable of replicating the behavior of the salt wedge as observed in the experiments.

5. Discussion

5.1. Inorganic Nitrogen Compounds in Upgradient Areas

In the following discussion we investigate the spatial distribution of nutrients in groundwater during the summer, when the nutrient concentrations near the shoreline were relatively high as shown in Figure 6. Figure 9 indicates spatially interpolated mean distributions of NO_3^-, NO_2^-, NH_4^+, and DO observed from August 7 to October 9. The upper layer in the aquifer near station 6 had relatively high DO concentrations ranging from 1.0 to 2.0 mg/L, a maximum nitrate concentration, and minima of nitrite and ammonium within the whole observational domain. Bacterial activity for nitrification is high in an aerobic aquifer and activates nitrification reactions of inorganic nitrogen compounds such as those shown by (10) and (11) [e.g., *Greenland and Hayes*, 1981]:

$$NH_4^+ + 3/2\ O_2 \leftrightarrow NO_3^- + H^+ + H_2O \qquad (10)$$

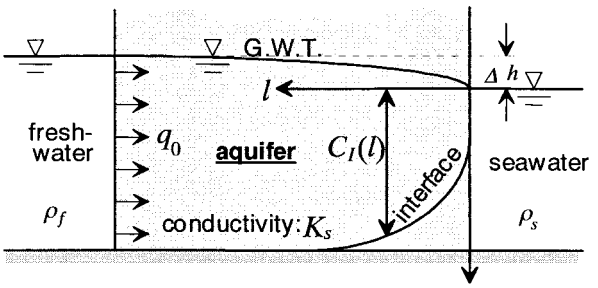

Figure 7. Definition sketch of the experimental formula of *Tamai and Shima* [1967].

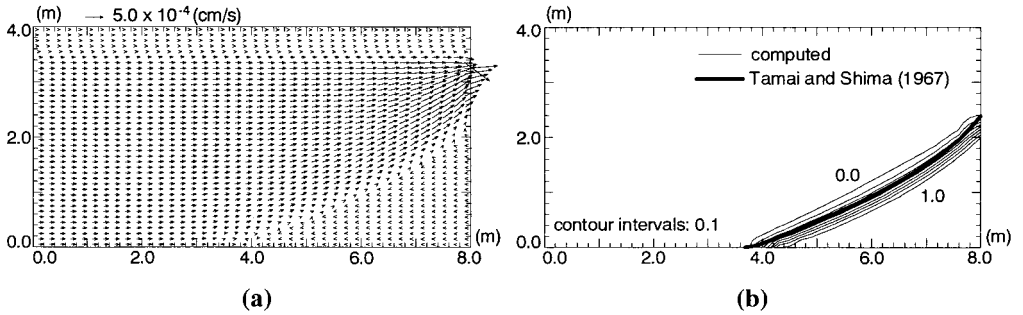

Figure 8. Computational results of (a) velocity field and (b) spatial distribution of nondimensional salinity. The thick curve in Figure 8b indicates the position of the interface calculated with the experimental formula of *Tamai and Shima* [1967].

$$NO_2^- + H_2O + 2\,Fe^{3+} \leftrightarrow NO_3^- + 2\,Fe^{2+} + 2\,H^+. \quad (11)$$

Nitrification corresponds to the oxidation reaction indicated by dextral arrows in the above equations. In contrast, denitrifying bacteria cause denitrification of inorganic nitrogen compounds in an anaerobic aquifer with organic carbon, i.e., (12) [e.g., *Freeze and Cherry*, 1979]:

$$CH_2O + 4/5\,NO_3^- \rightarrow 2/5\,N_2\,(gas) + HCO_3^- + 1/5\,H^+ + 2/5\,H_2O. \quad (12)$$

Nitrification and denitrification may not be completed to the last stage in which nitrogen compounds are entirely oxidized into nitrate or reduced to gaseous nitrogen, respectively. In that case, NO_2^-, NH_4^+, or N_2O (gas) are produced as intermediate compounds. These reactions are schematically displayed in Figure 10.

The upper groundwater layer in the upgradient area (station 6-a) was high in oxygen, and therefore appreciable nitrification could occur there with almost no denitrification. Thus the concentration of nitrate was high in the upper groundwater layer at station 6-a with little nitrite or ammonium present. On the contrary, DO decreased markedly to nearly zero in the lower groundwater layer at station 6-b where anaerobic conditions were correlated with a downward decrease in the nitrate concentration.

The observation at station 5 showed low values of nitrite and ammonium; levels roughly corresponded to those in the upper groundwater layer of station 6 inland. Although a higher oxygen concentration (nearly 3.5 mg/L) was detected in the upper layer at station 5, the nitrate concentration was only half of that in the upper layer at station 6. Such a decrease in the nitrate concentration could have been caused by microbial activity near roots of vegetation, which consumes nitrate and releases oxygen [*Freeze and Cherry*, 1979]. The pine tree vegetation is

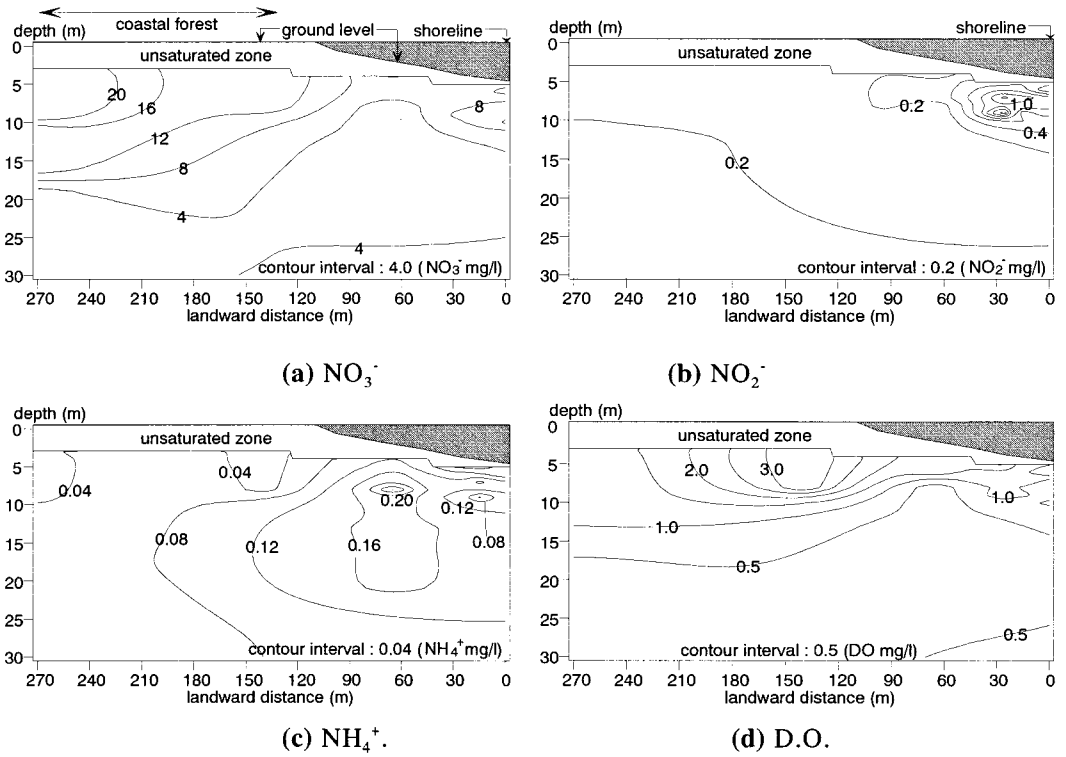

Figure 9. Spatial distributions of nitrate, nitrite, ammonium and DO concentration.

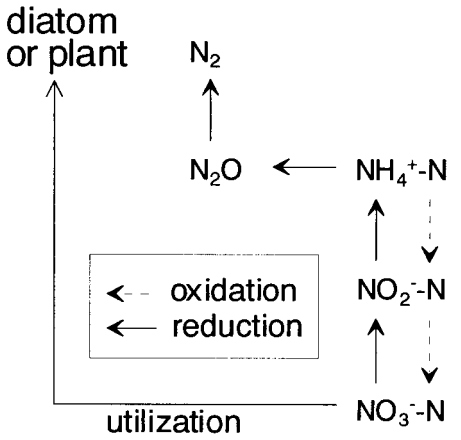

Figure 10. Schematic diagram of chemical reactions of inorganic nitrogen. Oxidation and reduction correspond to nitrification and denitrification, respectively.

hence considered to result in a higher utilization and removal of nitrate in the upper groundwater layers at station 5.

5.2. Inorganic Nitrogen Compounds on Beach

Although the concentrations of NO_3^- in the upper layer decreased from station 5 to 4, they increased toward station 1 near the shoreline (as shown in Figure 9) owing to nitrification under aerobic conditions at station 1. However, the concentrations of nitrite and ammonium also increased near the shoreline in spite of the existence of oxygen. This suggests that complicated biochemical reactions or mixing of deeper water with shallow water had occurred.

Sakamoto [1994] pointed out that dissolved organic nitrogen (DON) in seawater, which flows into and out of a coastal aquifer by tidal pumping, is decomposed and mineralized to ammonium in the aquifer and subsequently oxidized to nitrite and nitrate by nitrifying bacteria. Reduction (i.e., denitrification) to gaseous nitrogen by denitrifying bacteria does not normally take place in an aerobic aquifer at sandy shores. Therefore, mineralization of DON and the uptake of dissolved inorganic nitrogen (DIN) by bacteria determine the change in the total amount of DIN. On the other hand, *Lowrance and Pionke* [1989] reported that the active denitrifying bacteria could exist in an aquifer where aerobic and anaerobic conditions alternately arise from the groundwater table fluctuations due to tides. Moreover, a recent investigation by *Sumi and Ueda* [1997] suggested that significant numbers of denitrifying bacteria inhabit the aquifer near the shoreline and that denitrification can occur even in a sandy beach aquifer. The data acquired in the present survey show that the concentrations of nitrate, nitrite, and ammonium are high near the shoreline, and their highest concentrations among the data collected near the shoreline (stations 1–3) appear at station 2-b, which is located slightly landward of station 1 and just below the upper layer. These may suggest that in the aquifer near the shoreline, nitrification of DIN originated in the upgradient area coincides with mineralization of DON from seawater and that a portion of the nitrified DIN is subsequently denitrified to NO_2^- and NH_4^+. These reactions can be caused by denitrifying and nitrification bacteria, which activate with change of chlorine ion concentration and are the most vigorous in a brackish water [e.g., *Sumi and Ueda*, 1997]. Hence inorganic nitrogen is considered to experience the most notable biochemical reaction on the interface between seawater and fresh groundwater slightly below the seepage face near the shoreline. Detailed investigations have to be conducted to determine which mechanism is actually responsible.

Overall, we summarize that (1) DIN near the shoreline consists of a remarkably high nitrate concentration; (2) since sufficient oxygen is found in the inland aquifer, DIN appears to tend to be readily nitrified; and (3) the seaward transport of DIN by SGWD and the mineralization of DON, which may be followed by nitrification and denitrification, are considered to be responsible for the distribution of the inorganic nitrogen compounds in the aquifer near the shoreline.

5.3. Spatial Distribution of Phosphate and Silicate

The mean spatial distributions of PO_4^{3-} and SiO_2 during the summer are shown in Figure 11. Whereas relatively dilute phosphate appeared in the upgradient area, the aquifer near the shoreline had a high concentration of phosphate. The high concentration of phosphate near the shoreline may also have been caused by microbial decomposition and mineralization of dissolved organic phosphorus (DOP) supplied by seawater [*Hayashi*, 1979]. With the data obtained we were not able to determine exactly what mechanism caused the high concentration of phosphate near the shoreline. However, the data showed that the phosphate concentration declined from the summer to the autumn (Figure 6). Temperatures of seawater in Hasaki are typically 22°–24°C in summer and 15°–17°C in winter. These may support that DOP is supplied by seawater because rate of decomposition of DOP is reduced at lower water temperatures.

The concentration of silicate generally decreases from the

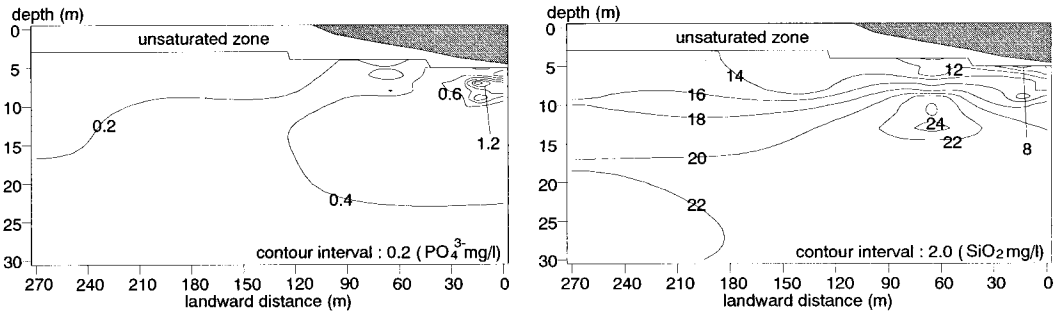

(a) PO_4^{3-} **(b)** SiO_2

Figure 11. Spatial distributions of phosphate and silicate concentration.

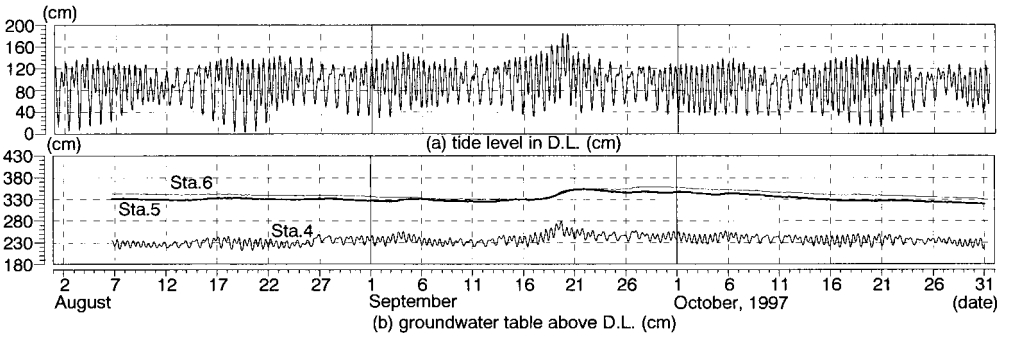

Figure 12. Time series of measured (a) tide level and (b) groundwater level at stations 4–6.

lower to upper groundwater layers and from the inland to the shoreline (except near station 4). Hence the primary silicate source is considered to be from the inland rather than from seawater.

5.4. Tidal Effects on Formation of the Saltwater Wedge

In order to estimate the groundwater velocity near the shoreline, fluctuation of seawater level due to tides and waves and groundwater table variation with precipitation should be included in the numerical simulation. Net groundwater flow may not be greatly influenced by waves, which require short time steps to simulate, and the simulation would become costly with waves included. Therefore we incorporated only the effects of variations of the groundwater table with tide and precipitation in the simulation. The model hence has been applied to simulate the formation of a saltwater wedge in the coastal aquifer and to investigate the effects of the tidal water table fluctuations.

Computations were performed for the two conditions, without (run 1) and with (run 2) the influence of the groundwater table fluctuations. The numerical simulations for both runs were made for 3 years; the last 3 months in run 2 corresponded to a part of the observational period, from August 1 to October 31. The linearly interpolated groundwater table elevation at the location 100 m inland of the shoreline (calculated from measured groundwater table elevations at stations 4 and 5 as shown in Figure 12) was applied to the landward boundary conditions of pressure potential ψ. Figure 12 also shows the time series of the tide and groundwater table data. In contrast, mean values of groundwater table elevation and tide level of August 22 at the boundaries were used in run 1; this means that steady salt wedge was computed in run 1.

Figures 13 and 14 show calculated results for runs 1 and 2 for velocity fields and nondimensional salinity distributions, both averaged over a day representative of August 22 in 1997. It can be seen from the velocity fields for both runs that freshwater outflow occurs as much as 40 m offshore and that the velocities near the seeping area are significantly higher than those of the interior domains. Whereas the discharge appears at a single area in run 1, the outflows in run 2 are found to occur at several areas near the shoreline with downward velocities in the upper layer of the aquifer beyond 40 m offshore.

The salinity distributions for runs 1 and 2 are appreciably different. The interface between seawater and fresh water was sharper in run 1; the dispersion width for run 2 was expanded. The upper part of the saltwater wedge in the aquifer for run 2 was inclined toward the upgradient area as well. These results are qualitatively consistent with the observed salinity distribution as shown in Figure 15 (note that the scales of cross-shore coordinates are different). The inclusion of the water table

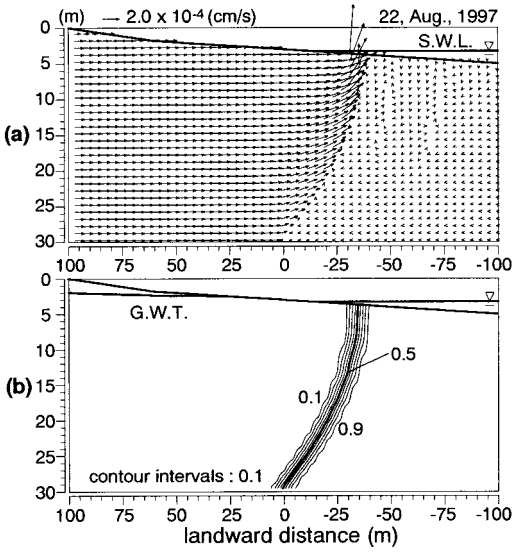

Figure 13. Computational results for run 1: spatial distribution of (a) velocity vectors and (b) nondimensional salinity.

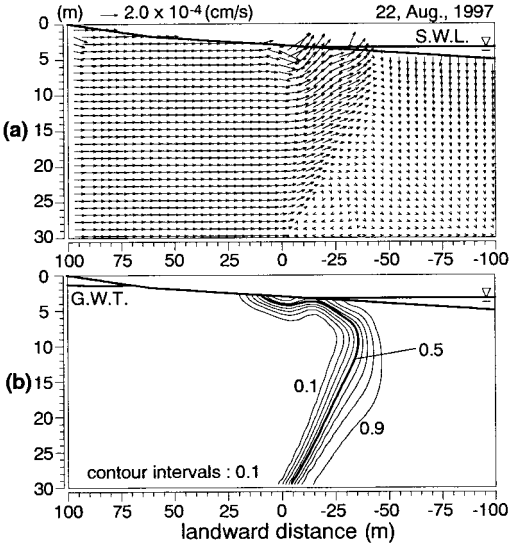

Figure 14. Computational results for run 2: spatial distribution of (a) velocity vectors and (b) nondimensional salinity.

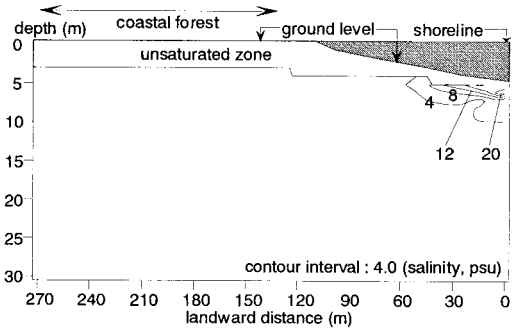

Figure 15. Spatial distribution of salinity measured on August 22, 1997.

fluctuations enables the model to reproduce the inclined salinity distribution near the shoreline. The water table fluctuations largely affect the flow and mass transport processes in the aquifer near the shoreline, where biochemical reaction has significant importance and nutrient distribution appreciably varies with depth. This effect hence must be incorporated in the simulation as accurately as possible.

5.5. Nutrient Fluxes Into the Sea by SGWD

To further investigate nutrient budgets in the shallow sea, the nutrient fluxes into the sea by SGWD were examined using the computed velocity field and the measured values of nutrient concentration in the aquifer near the shoreline. Table 2 lists the seaward nutrient fluxes caused by SGWD through the cross section at station 1 and by Tone River discharge [*Ministry of Construction*, 1994, 1995, 1996], both averaged over the whole observational period. An alongshore distance L of 16.0 km was used in the calculation of SGWD, and accordingly, the groundwater discharge ranged from 5.25×10^{-2} to 7.50×10^{-2} m^3/s. This distance corresponds to the natural uninterrupted coastline from the Tone River mouth in the south to the artificial Kashima port in the north. For the discharge of the Tone River the available data from 1993–1995 (in m^3/s) were used. In these 3 years the mean discharge was 212.2 m^3/s. The concentrations of NO_3^-, NO_2^-, NH_4^+, PO_4^{3-}, and SiO_2 were measured near the Tone River mouth. It can be seen from Table 2 that river discharge dominates nutrient supply to the Kashima Sea; the groundwater contribution is minor. However, since not all the nutrients released from the river mouth enter the study area, the results shown in Table 2 must be carefully interpreted. Satellite images show that the Tone River plume drifts mostly southward, and consequently, less direct nutrient supply to the Kashima Sea (north of Tone River mouth) is expected. Even though the river outflow is a major source of nutrients to the seawater in the Kashima Sea, its contribution to the shallow water environment may not be as high as that due to SGWD. The contribution of SGWD to the nutrient budget in the Kashima Sea thus should be discussed from other points of reference.

Table 2. Nutrient Fluxes by Groundwater Seeping and Tone River Discharge

	Groundwater, ton/d	Tone River, ton/d
NO_3^--N	0.0548	22.8673
NO_2^--N	0.0045	0.6485
NH_4^+-N	0.0047	3.6012
PO_4^{3-}-P	0.0078	1.3496
SiO_2-Si	0.4351	11.9039

The nearshore circulation cells, which were modeled by *Inman et al.* [1971], produce a continuous interchange of water between the surf zone and the offshore zone. Nutrient transport processes in the nearshore shallow sea can be represented as shown schematically in Figure 16. The cells act as distributing and dispersing mechanisms for land runoff and other materials injected into the surf zone. Nutrients from SGWD introduced into the surf zone are carried along the shore, strongly mixed with the water in the surf zone by turbulence of wave breaking, and transported by the seaward flowing rip currents through the cross section B-B′. The water subsequently spreads over the "secondary mixing zone" from the rip heads, being transported into the surf zone by onshore mass transport due to waves. Therefore the nearshore circulation cells horizontally mix the water of the surf zone with that of the secondary mixing zone.

Another mixing mechanism occurs in the outer part of the surf zone. Onshore mass transport due to wave action and offshore return flow result in the water interchange between the secondary mixing zone and the offshore zone at the cross section A-A′. Assuming a wave period of 7.0 s and wave height of 1.2 m representative of normal wave condition in the Kashima Sea [e.g., *Nagai et al.*, 1999], we estimated the onshore mass transport with second-order accuracy to be Q_o =

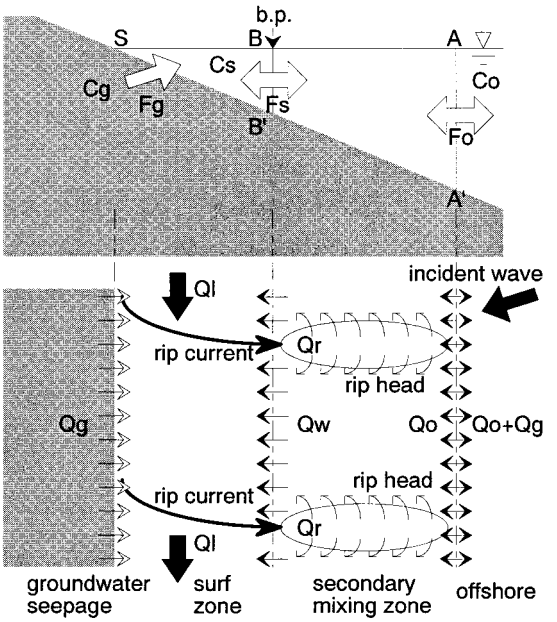

Figure 16. Schematic diagram of a mixing in the surf zone based on the model of *Inman et al.* [1971]. The zone between rip currents constitutes a circulation cell. The b.p. and S in the top indicate a breaking point and a shoreline. Q_o, Q_w, Q_r, Q_l, and Q_g are volume fluxes per unit width caused by onshore mass transport through the cross section A-A′, onshore mass transport through B-B′, rip current through B-B′, alongshore current, groundwater flow seeping near the shoreline, respectively. F_g, F_o, and F_s are nutrient fluxes provided by groundwater at discharge zone, offshore water at A-A′, and water in the secondary mixing zone at B-B′ over the alongshore distance L. C_g, C_o, and C_s are nutrient concentrations in groundwater, offshore seawater, and nearshore seawater.

2.24×10^{-2} (m^2/s) at A-A′. In addition, the volume flux per unit width caused by rip currents through the cross section B-B′ is $Q_r = 9.43 \times 10^{-2}$ (m^2/s) according to *Inman et al.* [1971] on the assumption that the width and the seabed slope of the surf zone are 150 m and 1/50, respectively. The averaged volume flux per unit width of groundwater flow was calculated as $Q_g = 3.93 \times 10^{-5}$ (m^2/s) based on the numerical simulations.

To analyze the mixing in the surf zone and the secondary mixing zone, we shall apply a "box" model to the water body consisting of these two zones. If the flow and nutrient fields in the alongshore direction are uniform, the budget of nutrient fluxes in the box can be expressed as follows:

$$V(dC_s/dt) = F_g + F_o, \tag{13}$$

where V is the volume of the box, C_s is the nutrient concentration in the box, and F_g and F_o are the nutrient fluxes provided by the groundwater and the offshore water over the alongshore distance L. Considering $Q_g \ll Q_o$, F_o is calculated by (14),

$$F_o = L\{Q_oC_o - (Q_o + Q_g)C_s\} \cong L(Q_oC_o - Q_oC_s), \tag{14}$$

where C_o is the nutrient concentration in the offshore water. We can rewrite (13) as

$$V(dC_s/dt) = F_g + LQ_o(C_o - C_s). \tag{15}$$

The solution for (15) is readily obtained as

$$C_s = \left(\frac{F_g}{LQ_o} + C_o\right)\left\{1 - \exp\left(-\frac{LQ_o}{V}t\right)\right\} + C_{s0}\exp\left(-\frac{LQ_o}{V}t\right), \tag{16}$$

where C_{s0} is the value of C_s at the time $t = 0$. The first term on the right-hand side of (16) represents rise of concentration due to inflow of groundwater and offshore water, and the second term shows decline of concentration caused by outflow from the box to the offshore. The value of C_s therefore approaches $(F_g/LQ_o + C_o)$ at $t \to +\infty$.

The area of the cross section of the box, S, is estimated with the seabed slope of 1/50 and a width of the secondary mixing zone of 270 m (1.8 times the surf zone width [cf. *Inman et al.*, 1971]). The volume of the box, $V = SL$, divided by LQ_o gives ~21.9 hours, which is the residence time in the box for nutrients from the groundwater. This means that the nutrients discharged by SGWD are expected to stay in the box for almost 1 day. Figure 17 indicates the temporal variations of the concentration C_s of nitrate and both the terms on the right-hand side of (16). The offshore water concentration C_o and the initial concentration C_{s0} are set in the calculation of (16) to be 0.0 and 0.0653 mg/L (the measured value of the mean nitrate concentration of the seawater). The condition of $C_o = 0.0$ assumed here is preconceived to result in noticeable dilution. The nitrate concentration C_s actually appears to fall immediately in a few days and finally to approach F_g/LQ_o, 1.77×10^{-3} mg/L, as shown in Figure 17. The values of F_g/LQ_o hence are significant for estimating the contribution of SGWD to the nutrient concentration in the nearshore water with the influence of mixing of the seawater in the surf zone. The averaged concentration C_s of five compounds in the water near the shoreline are listed in Table 3 with F_g/LQ_o and the ratios of F_g/LQ_o to C_s. The ratios ranging from 0.331 to 3.035% imply that SGWD plays a minor role in the nutrient budget of the nearshore water in the Hasaki area.

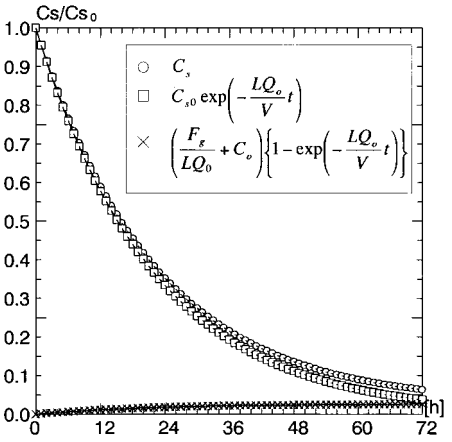

Figure 17. Nutrient concentration C_s as a function of time with $C_o = 0.0$. The circles, squares, and crosses represent C_s and second and first terms on the right-hand side of (16), respectively.

Table 3. Averaged Shallow Water Nutrient Concentration C_s, F_g/LQ_0 Denoting the Effect of SGWD on Shallow Water Nutrient Concentration, and the Ratio of F_g/LQ_0 to C_s

	C_s, mg/L	F_g/LQ_0, mg/L	Ratio, %
NO_3^--N	0.0653	1.77×10^{-3}	2.710
NO_2^--N	0.0089	1.45×10^{-4}	1.633
NH_4^+-N	0.0458	1.52×10^{-4}	0.331
PO_4^{3-}-P	0.0083	2.52×10^{-4}	3.035
SiO_2-Si	0.4867	1.41×10^{-2}	2.887

On the contrary, Tone River, which has the largest drainage basin in Japan and a proportionally large amount of discharge, provides enormous nutrient fluxes as shown in Table 2. In a coastal area with less river influence, nutrient inputs due to SGWD may be more significant than that in the study area.

Although the calculations of nutrient fluxes were based on the assumption that the aquifer consists of homogeneous sand, pipe flow through macropores is believed to affect dewatering of groundwater, as is discussed in the area of hillslope hydrology. Furthermore, outfalls, irrigation channels, and streams, which can be seen in the field, probably introduce nutrient-rich water directly into the nearshore sea. These nutrient supplies should be considered in analyses of nutrient budgets in future work.

6. Conclusion

Groundwater at Hasaki Beach, which is located in an intensively cultivated agricultural area, generally has high concentrations of inorganic nutrients compared with seawater and river water. During summer, nitrification produces high nitrate concentrations in the landward upper aquifer under aerobic conditions, while nitrite and ammonium concentrations are low. The aquifer near the shoreline is a complex chemical environment in which denitrification and nitrification simultaneously or alternately occur. Moreover, SGWD from the up-

gradient area and decomposition and mineralization of organic matter from the sea is considered to supply inorganic nutrients to this part of the aquifer; those are mixed together and then transported into the sea. The microbial activity related to biochemical processes in the aquifer near the foreshore zone varies seasonally as evident in the seasonal changes of the nutrient concentrations.

With the effects of groundwater table and tidal fluctuations included, a numerical model was used to estimate the nutrient fluxes from the aquifer into the sea on the assumption that the aquifer consists of homogeneous sandy soil. The nutrient fluxes from SGWD are found to be minor as compared with the nutrient flux from Tone River. Additionally, according to the results of box model analysis, the nutrient fluxes due to SGWD have little influence on the shallow water ecosystem around the surf zone in this area.

SGWD, however, may be underestimated since pipe flow through macropores and effects of wave run-up and setup are neglected in the computations. Therefore further investigations are needed, including a field survey and the improvement of the numerical model to clarify the importance of these effects.

Acknowledgments. The first author wishes to thank Y. Kuriyama of the Port and Harbour Research Institute, Yokosuka, Japan, and L. Li of the University of Edinburgh, Edinburgh, U.K., for their helpful comments on the manuscript. We are grateful to T. Nakasone (National Research Institute of Fisheries Engineering, Hasaki, Japan) for his help with the field measurements.

References

Apello, C. A. J., and D. Postma, *Groundwater and Pollution*, A. A. Balkema, Brookfield, Vt., 1993.

Bear, J., *Dynamics of Fluids in Porous Media*, Dover Sci., New York, 1972.

Brooks, R. H., and A. T. Corey, Properties of porous media affecting fluid flow, *J. Irrig. Drain Eng.*, *92*, 61–88, 1966.

Capone, D. G., and M. F. Bautista, A groundwater source of nitrate in nearshore marine sediments, *Nature*, *313*, 214–216, 1985.

Church, T. M., An underground route for the water cycle, *Nature*, *380*, 579–580, 1996.

Cooper, H. H., A hypothesis concerning the dynamic balance of freshwater and saltwater in a coastal aquifer, *J. Geophys. Res.*, *64*, 461–467, 1959.

D'Elia, C. F., K. L. Webb, and J. W. Porter, Nitrate-rich groundwater inputs to Discovery Bay, Jamaica: A significant source of N to local reefs?, *Bull. Mar. Sci.*, *31*, 903–910, 1981.

Emery, K. O., and J. F. Foster, Water tables in marine beach, *J. Mar. Res.*, *7*, 644–654, 1948.

Freeze, R. A., and J. A. Cherry, *Groundwater*, Prentice-Hall, Englewood Cliffs, N. J., 384–457, 1979.

Glover, R. E., The pattern of freshwater flow in a coastal aquifer, *J. Geophys. Res.*, *64*, 457–459, 1959.

Greenland, D. J., and M. H. B. Hayes, *The Chemistry of Soil Processes*, John Wiley, New York, 1981.

Hayashi, K., Purification by sandy beach (in Japanese), in *Self Purification and Acceleration of Purification in Water Regions*, pp. 111–124, Kouseisha-Kouseikaku, Tokyo 1979.

Inman, D. L., R. J. Tait, and C. E. Nordstrom, Mixing in the surf zone, *J. Geophys. Res.*, *76*, 3493–3514, 1971.

Irmay, S., On the hydraulic conductivity of unsaturated soils, *Eos Trans. AGU*, *35*, 463–467, 1954.

Johannes, R. E., The ecological significance of the submarine discharge of groundwater, *Mar. Ecol. Prog. Ser.*, *3*, 365–373, 1980.

Kimura, T., I. Hayami, and S. Yoshida, *Geology of Japan*, Univ. of Tokyo Press, Tokyo, 1991.

Kohno, I., M. Nishigaki, and S. Tanaka, Finite element analysis of transient intrusion of saline water in saturated-unsaturated seepage (in Japanese), *Proc. Jpn. Soc. Civ. Eng.*, *331*, 133–141, 1983.

Kohout, F. A., The flow of fresh water and salt water in the Biscayne Bay aquifer of the Miami area, Florida: Sea water in coastal aquifers, *U.S. Geol. Surv. Water Supply Pap.*, *1616-C*, 12–32, 1964.

Kohout, F. A., and M. C. Kolipinski, Biological zonation related to groundwater discharge along the shore of Biscayne Bay, Miami, Florida, in *Estuaries*, edited by G. H. Lauff, pp. 488–499, Am. Assoc. Adv. Sci., Washington, D. C., 1967.

Li, L., D. A. Barry, J. Y. Parlange, and C. B. Pattiaratchi, Beach water table fluctuations due to wave run-up: Capillary effects, *Water Resour. Res.*, *33*, 935–945, 1997a.

Li, L., D. A. Barry, and C. B. Pattiaratchi, Numerical modeling of tide-induced beach water table fluctuations, *Coastal Eng.*, *30*, 105–123, 1997b.

Lowrance, R. R., and H. B. Pionke, Transformation and movement of nitrate in an aquifer systems, in *Nitrogen Management and Groundwater Protection*, edited by R. F. Follett, pp. 373–392, Elsevier Sci., New York, 1989.

Manheim, F. T., Evidence for submarine discharge of water on the Atlantic continental slope of the southern United States, and suggestions for further search, *Trans. N. Y. Acad. Sci.*, *Ser. II*, *28*, 839–853, 1967.

Marsh, J. A., Jr., Terrestrial inputs of nitrogen and phosphates on fringing reefs on Guam, *Proceedings: Third International Coral Reef Symposium*, pp. 331–336, Univ. of Miami, Miami, Fla., 1977.

McLachlan, A., and W. Illenberger, Significance of groundwater nitrogen input to a beach/surf zone ecosystem, *Stygologia*, *2*(4), 1986.

Ministry of Construction, Annual report on river discharge 1993 (in Japanese), Tokyo, 1994.

Ministry of Construction, Annual report on river discharge 1994 (in Japanese), Tokyo, 1995.

Ministry of Construction, Annual report on river discharge 1995 (in Japanese), Tokyo, 1996.

Momii, K., K. Jinno, T. Ueda, T. Itoh, T. Hosokawa, and F. Hirano, Numerical analysis on saltwater intrusion and dispersion in an unsaturated-saturated coastal aquifer (in Japanese), *J. Groundwater Hydrol.*, *28-3*, 103–112, 1986.

Moore, W. S., Large groundwater inputs to coastal waters revealed by ^{226}Ra enrichments, *Nature*, *380*, 612–615, 1996.

Nagai, T., K. Sato, K. Sugahara, and K. Kawaguchi, Annual Report on NOWPHAS 1997 (in Japanese), *Tech. Note 926*, pp. 253–258, Port and Harbor Res. Inst., Yokosuka, Japan, 1999.

Nielsen, D., and G. Yeates, A comparison of sampling mechanism available for small-diameter groundwater monitoring wells, *Ground Water Monit. Rev.*, *2-2*, 83–99, 1985.

Nielsen, P., Tidal dynamics of the water table in beaches, *Water Resour. Res.*, *26*, 2127–2134, 1990.

Nielsen, P., and S. L. Dunn, Manometer tubes for coastal hydrodynamics investigations, *Coastal Eng.*, *35*, 73–84, 1998.

Parlange, J. Y., and W. Brutsaert, A capillary correction for free surface flow of groundwater, *Water Resour. Res.*, *20*, 805–808, 1987.

Pinder, G. F., and H. H. Cooper Jr., A numerical technique for calculating the transient position of the saltwater front, *Water Resour. Res.*, *6*, 875–882, 1970.

Pinder, G. F., and W. G. Gray, *Finite Element Simulation in Surface and Subsurface Hydrology*, Academic, San Diego, Calif., 1977.

Raghunath, H. M., *Ground Water: Hydrogeology, Ground Water Survey, and Pumping Tests, Rural Water Supply and Irrigation Systems*, John Wiley, New York, 1982.

Richards, L. A., Capillary conduction of liquids through porous mediums, *Physics*, *1*, 318–333, 1931.

Rigg, C. O., and A. W. Hatheay, Groundwater monitoring field practice—An overview, in *Groundwater Contamination: Field Methods*, pp. 121–136, Am. Soc. for Test. Mater., Philadelphia, Pa., 1988.

Sakamoto, I., Tidal respiration (or the aerobic decomposition and recycling with surf water) in the sandy beach (in Japanese), *J. Water Waste*, *36-1*, 44–52, 1994.

Scheidegger, A. E., General theory of dispersion in porous media, *J. Geophys. Res.*, *66*, 3273–3278, 1961.

Segol, G., G. F. Pinder, and W. G. Gray, A galerkin-finite element technique for calculating the transient position of the saltwater front, *Water Resour. Res.*, *11*, 347–353, 1975.

Simmons, G. M., Jr., Importance of submarine groundwater discharge (SGWD) and seawater cycling to material flux across sediment/water interfaces in marine environments, *Mar. Ecol. Prog. Ser.*, *84*, 173–184, 1992.

Sumi, E., and S. Ueda, Inflow processes of nutrients in coastal aquifer

toward the nearshore water, paper presented at the 5th Symposium for Groundwater Contamination, Jpn. Soc. of Civ. Eng. Tokyo, 1997.
Sutcliffe, W. H., Some relations of land drainage, nutrient and particulate material, and fish catches in two eastern Canadian bays, *Can. J. Fish. Aquat. Sci*., *29*, 357–362, 1972.
Tamai, N., and S. Shima, Salt-water wedge in unconfined coastal aquifers, *Trans. Jpn. Soc. Civ. Eng*., *139*, 31–38, 1967.
Tani, H., Characteristics of surface water rising due to vertical one dimensional unsaturated flow, *J. For*., *64*, 409–418, 1982.
Turner, I., Water table outcropping on macro-tidal beaches: A simulation model, *Mar. Geol*., *115*, 227–238, 1993.
Younger, P. L., Submarine groundwater discharge, *Nature*, *382*, 121–122, 1996.

K. Adachi, National Research Institute of Fisheries Engineering, Ebidai, Hasaki, Ibaraki 314-0421, Japan.

K. Nadaoka and P. Rölke, Graduate School of Information Science and Engineering, Tokyo Institute of Technology, 2-12-1 O-okayama, Meguro-ku, Tokyo 152-8552, Japan.

Y. Uchiyama, Marine Environment Division, Port and Harbour Research Institute, 3-1-1 Nagase, Yokosuka 239-0826, Japan. (uchiyama@ipc.phri.go.jp)

H. Yagi, Department of Civil Engineering, Tokyo Institute of Technology, 2-12-1 O-okayama, Meguro-ku, Tokyo 152-8552, Japan.

(Received February 1, 1999; revised January 24, 2000; accepted February 7, 2000.)